THE JOURNAL OF BIOLOGICAL CHEMISTRY
Vol. 278, No. 45, Issue of November 7, pp. 44496–44504, 2003
Printed in U.S.A.


# Essential Roles of Zinc Ligation and Enzyme Dimerization for Catalysis in the Aminoacylase-1/M20 Family*

Received for publication, April 22, 2003, and in revised form, August 21, 2003
Published, JBC Papers in Press, August 21, 2003, DOI 10.1074/jbc.M304233200

**Holger A. Lindner‡, Vladimir V. Lunin, Alain Alary, Regina Hecker, Miroslaw Cygler, and Robert Ménard**

*From the Biotechnology Research Institute, National Research Council of Canada, Montréal, Québec H4P 2R2, Canada*

**Members of the aminoacylase-1 (Acy1)/M20 family of aminoacylases and exopeptidases exist as either monomers or homodimers. They contain a zinc-binding domain and a second domain mediating dimerization in the latter case. The roles that both domains play in catalysis have been investigated for human Acy1 (hAcy1) by x-ray crystallography and by site-directed mutagenesis. Structure comparison of the dinuclear zinc center in a mutant of hAcy1 reported here with dizinc centers in related enzymes points to a difference in zinc ligation in the Acy1/M20 family. Mutational analysis supports catalytic roles of zinc ions, a vicinal glutamate, and a histidine from the dimerization domain. By complementing different active site mutants of hAcy1, we show that catalysis occurs at the dimer interface. Reinterpretation of the structure of a monomeric homolog, peptidase V, reveals that a domain insertion mimics dimerization. We conclude that monomeric and dimeric Acy1/M20 family members share a unique active site architecture involving both enzyme domains. The study may provide means to improve homologous carboxypeptidase G2 toward application in antibody-directed enzyme prodrug therapy.**

Zinc peptidases play roles in metabolic and signaling pathways throughout all kingdoms of life. A growing number of these enzymes have been found to contain two zinc ions at their active sites. Some are regarded as potential pharmaceutical targets (1). Recently, Wouters and Husain (2) pointed out that members of the MH and MF clans[1] of dizinc peptidases, together with the MC clan of monozinc peptidases display three different catalytic zinc centers that have evolved in a similar structural scaffold, which is exemplified by carboxypeptidase A of clan MC. Although they all appear to employ the same general base-like catalytic mechanism, neither all catalytic residues nor the substrate-binding sites are conserved among the three clans. A glutamate residue representing a putative catalytic base, for instance, resides in different regions of the polypeptide chain in the MH and MC clans. In the MF clan enzyme leucine aminopeptidase, a bicarbonate ion replaces the glutamate residue. Moreover, whereas the monozinc center in the MC clan is structurally equivalent to one of the two zinc-binding sites in the dinuclear zinc center in the MH clan, it does not share any homology with the dinuclear zinc center in the MF clan anymore. As a consequence, members of families from each clan must be examined individually in order to gain a detailed understanding of their catalytic machineries.

Aminoacylase-1 (Acy1[2]; EC 3.5.1.14) was discovered in 1881 by virtue of its ability to hydrolyze hippuric acid in crude kidney homogenates (4) and is now classified in the M20 family of clan MH, also referred to as the Acy1 family (5). Acy1 plays a general role in the cytosolic breakdown of $N^{\alpha}$-acetylated amino acids (6) generated during protein degradation (7). Other functional aminoacylase enzymes from the Acy1/M20 family (Table I) are implicated in the bacterial biosynthesis pathways of arginine (*N*-acetylornithine deacetylase), lysine, and the cell wall (succinyldiaminopimelate desuccinylase) (8). Several enzymes of the Acy1/M20 family are known as exopeptidases (Table I). They include CPG2 (9–11), *Saccharomyces cerevisiae* carboxypeptidase Y (12), PepT and the dipeptidase enzyme PepV from various bacterial sources (13–15), *Escherichia coli* X-His dipeptidase (16), and human nonspecific dipeptidase and a brain-specific carnosinase that possibly plays a role in aging and neurodegenerative or psychiatric diseases (17). The enzymatic function of a related drought-induced polypeptide-1 from wild watermelon (*Citrullus lanatus*) remains unknown (18).

Enzymes of the Acy1/M20 family have shown potential for different applications. In biocatalysis, the high stereoselectivity of Acy1 allows the preparation of L-amino acids from racemic mixtures of *N*-acyl-L-amino acids (19). Succinyldiaminopimelate desuccinylase is considered as a potential anti-bacterial target (1), and CPG2 is considered a therapeutic agent in ADEPT for cancer treatment (18). However, compared with the well characterized active sites of AAP (21) and SGAP (22) from the M28 family of clan MH (Table I), relatively little is known about the Acy1/M20 family. The crystal structures of two Acy1 homologs, CPG2 (23) and PepT from *Salmonella typhimurium* (24), are each folded into a metal-binding domain and a smaller dimerization domain, which is inserted in the middle of the sequence of the metal-binding domain. In the structures of both enzymes, the two domains display an open conformation. Porcine Acy1 was shown by limited proteolysis to have a closely similar domain structure (25, 26). The metal-binding domains in CPG2 and PepT exhibit high structural similarity to the two single-domain proteins AAP and SGAP

* This is National Research Council of Canada publication 46160. The costs of publication of this article were defrayed in part by the payment of page charges. This article must therefore be hereby marked "*advertisement*" in accordance with 18 U.S.C. Section 1734 solely to indicate this fact.

‡ To whom correspondence should be addressed: Biotechnology Research Institute, National Research Council of Canada, Montréal, Québec H4P 2R2, Canada. Tel.: 514-496-1887; Fax: 514-496-5143; E-mail: Holger.Lindner@cnrc-nrc.gc.ca.

[1] This report follows the MEROPS classification of peptidases (available on the World Wide Web at merops.sanger.ac.uk) (3). This system groups peptidases with significant sequence similarity into a family and assigns families of common evolutionary origin to a clan.

[2] The abbreviations used are: Acy1, aminoacylase 1; CPG2, *Pseudomonas* sp. carboxypeptidase G2; PepT, amino tripeptidase T; PepV, peptidase V; ADEPT, antibody-directed prodrug therapy; AAP, *Aeromonas proteolytica* aminopeptidase; SGAP, *Streptomyces griseus* aminopeptidase; hAcy1, human Acy1; r.m.s., root mean square.

TABLE I
*Representative enzymes of the M20 and M28 families*

| Enzyme | MEROPS identifier[a] |
|---|---|
| *N*-Acylamino acid amidohydrolases | |
| Human aminoacylase-1 (L-acylamino acid amidohydrolase) | M20.973 |
| Bacterial *N*-acetylornithine deacetylase | M20 nonpeptidase homologue |
| Bacterial succinyldiaminopimelate desuccinylase | M20 nonpeptidase homologue |
| Carboxypeptidases | |
| *Pseudomonas* sp. carboxypeptidase G2 | M20.001 |
| *S. cerevisiae* carboxypeptidase Y | M20.002 |
| Human glutamate carboxypeptidase II | M28.010 |
| Amino tripeptidases and dipeptidases | |
| Bacterial amino tripeptidase T | M20.003 |
| Bacterial peptidase V | M20.004 |
| *E. coli* X-His dipeptidase | M20.007 |
| Human nonspecific dipeptidase | M20.005 |
| Human carnosinase | M20.006 |
| *A. proteolytica* aminopeptidase | M28.002 |
| *S. griseus* aminopeptidase | M28.003 |
| Specificity unknown | |
| *Citrullus lanatus* drought-induced polypeptide | M20 nonpeptidase homologue |

[a] The first part of the MEROPS identifier indicates the family assignment.

and are thought to be responsible for catalysis. Besides CPG2 and PepT, numerous other members of the Acy1/M20 family, including Acy1, appear to exist as homodimers (8, 17, 26–28). It is not clear whether the dimerization domain in these enzymes is involved in catalysis.

Recently, the crystal structure of PepV from *Lactobacillus delbrueckii* revealed that the enzyme exists as a monomer (29). As in the dimer forming enzymes of the Acy1/M20 family, the additional domain in PepV is inserted in the zinc-binding domain and is referred to as the lid domain. The structure of PepV was determined in a complex with an inhibitor, Asp$\Psi$[$PO_2CH_2$]AlaOH, which mimics the transition state of a dipeptide substrate, bound in a hydrophobic cavity between the zinc-binding and the lid domain (29). Its interactions with the enzyme pinpoint the active site residues. In addition to residues from the zinc-binding domain, residues from the lid domain also appear to be involved in substrate binding and catalysis.

Here, we report the crystal structure of the metal-binding domain of a mutant of hAcy1. A spatial comparison of MH clan enzymes showed high structural conservation of the dinuclear zinc center but also revealed a difference in zinc ligation, which correlates with differences in substrate specificity among the known enzymes of the Acy1/M20 family. Mutational studies of hAcy1 suggest that both zinc sites and a conserved glutamate in their immediate vicinity are essential for catalysis. We further recognized that the lid domain in the related but monomeric enzyme PepV mimics the structure of a dimer and thereby inserts a catalytic histidine into the active site. Mutational analysis of the corresponding histidine in the small domain of hAcy1 supports the role of this residue in catalysis in the dimeric enzyme. An enzyme complementation assay provides evidence that the histidine is acting *in trans* and that catalysis occurs at the dimer interface.

## EXPERIMENTAL PROCEDURES

*Site-directed Mutagenesis*—Site-directed mutagenesis was performed on the baculovirus transfer vector pVL1393-hAcI (30) using the QuikChange™ XL site-directed mutagenesis kit (Stratagene). Forward versions of the mutagenic primers are listed in Table II. The sequences of the mutant hAcy1 genes in the resulting transfer vectors were confirmed by DNA sequencing.

*Enzyme Expression and Purification*—Wild-type hAcy1 and its variants were expressed in a baculovirus expression vector system and purified as described (30). In brief, 300-ml cultures of infected Sf21 cells were harvested 72 h after infection. A two-step purification protocol was applied in all cases. The enzyme preparations were stored at −80 °C. Before use, protein samples were transferred into the appropriate buffer using a PD-10 column (Amersham Biosciences). Protein was concentrated using Centricon-10 concentrators (Amicon) following the instructions of the supplier. Protein concentrations were determined by the Bradford assay (31) with bovine serum albumin as the standard.

*Protein Crystallization, Data Collection, and Refinement*—Crystals were obtained by the hanging drop vapor diffusion method, equilibrating drops containing 1.5 $\mu$l of protein (5–8 mg/ml) in 20 mM Tris-HCl buffer, pH 7.5, and 2.0 $\mu$l of reservoir solution (20% (w/v) polyethylene glycol 8000, 0.2 M $(NH_4)_2SO_4$, 2 mM $CoCl_2$, and 10 mM norleucine) suspended over 1.0 ml of reservoir solution. The crystals belong to the space group $P2_12_12_1$ with unit cell dimensions $a$ = 53.53 Å, $b$ = 67.23 Å, $c$ = 146.48 Å and two molecules forming a dimer in the asymmetric unit. Dissolved protein crystals were analyzed by SDS-PAGE, showing protein bands at 25 and 12 kDa (not shown), whereas the full form of the protein is 46 kDa. The remaining 9-kDa fragment was not detectable. Prior to data collection, the crystals were soaked in a cryo-protecting solution of 25% (w/v) polyethylene glycol 8000, 0.2 M $(NH_4)_2SO_4$, 22.5% (v/v) glycerol and were flash cooled in a cold stream of $N_2$ gas to 100 K. Diffraction data sets for all crystals were collected using a Quantum-4 CCD detector at the X8C beamline, NSLS, Brookhaven National Laboratory (Table III). Data processing and scaling for all data sets were performed with the program HKL2000 (32).

The protein structure was determined by SIRAS phasing using a native data set and the anomalous peak wavelength from a Hg derivative, obtained by overnight soaking in reservoir solution, containing 2 mM thimerosal. Four Hg sites in the asymmetric unit were found using the program SOLVE (33). The phases calculated to 1.5 Å with these sites gave an overall figure of merit of 0.25. Electron density modification was applied with the program RESOLVE (34) with the solvent content set to 0.4. The figure of merit after density modification was 0.51 at 1.5 Å. Approximately 95% of the protein main chain was built automatically with the ARP/WARP package (35) in warpNtrace mode with input experimental phases after RESOLVE. Side chains were inserted using the docking routine from the ARP/WARP package. The model was then adjusted manually using the program O (36) and refined against a native data set using the program REFMAC version 5.1.08 (37) in anisotropic mode with no $\sigma$ cut-off. During refinement, 1% of the reflections were set aside for the calculation of $R_{free}$. Water molecules were initially added automatically with CNS (38) and subsequently by visual inspection of difference maps. The final model has been refined to a R-factor of 0.133 and $R_{free}$ of 0.172 at 1.4 Å (Table IV). The model was further analyzed with the program PROCHECK (39), which showed that 88.9% of all residues are in the most favored regions, 10.6% are in additionally allowed regions, two residues are in generally allowed regions, and none in a disallowed region of the Ramachandran plot. All stereochemistry parameters checked by PROCHECK are "inside" or "better" compared with the standard values and deviations.

*Assays of Enzyme Activity and Stability*—Acy1 activity was determined at pH 7.4 by a discontinuous colorimetric assay as described before (30). Kinetic data were evaluated by nonlinear regression analysis using both the Michaelis-Menten equation ($v = V_{max} \times [S]/(K_m + [S])$) and the Hill equation ($v = V_{max} \times [S]^n/([S]_{0.5}{}^n + [S]^n)$), where $[S]_{0.5}$ represents the substrate concentration at half-saturation, and the Hill coefficient, $n$, is a quantitative measure of cooperativity. The catalytic constant, $k_{cat}$, was calculated using the equation $V_{max} = k_{cat} \times [E]$, where $[E]$ represents total enzyme concentration. Kinetic parameters were taken from the equation that generated the best fit to experimental data.

As a measure of stability, the "melting temperature," $T_m$, and the denaturation energy, $\Delta G(H_2O)$, of each enzyme variant were determined as described previously (26). $T_m$ values were acquired by monitoring enzymatic inactivation during the slow heating of samples. Aliquots were withdrawn at regular intervals and subjected to enzyme activity determinations. $\Delta G(H_2O)$ values were estimated by fluorescence equilibrium denaturation on an SPEX Fluorolog-2 spectrofluorometer, using guanidine hydrochloride as the denaturant.

*Structure-based Alignment and Structure Comparison*—Structure-based sequence alignments were derived manually for the zinc-binding domain in the T347G mutant of hAcy1,[3] and representative structures

[3] The atomic coordinates for the crystal structure of this protein are available in the Protein Data Bank (http://www.rcsb.org/pdb) under PDB number 1Q7L (40).

TABLE II
*Forward versions of mutagenic primers*

| Mutant | Predicted role in hAcy1 | Oligonucleotide sequence[a] |
|---|---|---|
| E148A | Zinc binding | 5′-GCCTGATGAGGCGGTTGGGGGTCACC-3′ |
| H373A | Zinc binding | 5′-CCTGTGCTGCTGGCCGACCACGATGAACGGC-3′ |
| H80A | Zinc binding | 5′-CTCAACTCCGCCACGGATGTGGTGCCTGTCTTCAAG-3′ |
| E175A | Zinc binding | 5′-GGCTTTGCCCTGGATGCGGGCATAGCCAATCC-3′ |
| D113A | Zinc binding | 5′-GGGGTGCCCAGGCCATGAAGTGCGTCAGC-3′ |
| E147A | General base | 5′-CCTTTGTGCCTGATGCGGAGGTTGGGGG-3′ |
| E147Q | | 5′-CCTTTGTGCCTGATCAGGAGGTTGGGGG-3′ |
| E147D | | 5′-CCTTTGTGCCTGATGACGAGGTTGGGGG-3′ |
| H206N | Catalytic | 5′-GGGAGGCCAGGCAATGCCTCACGCTTC-3′ |
| T347G | | 5′-GCCTGCTGCCGGTGACAACCGCTATATCCG-3′ |

[a] Altered nucleotides are underlined.

TABLE III
*X-ray diffraction data collection statistics*

| Data set | Hg-Peak | Native |
|---|---|---|
| Wavelength | 1.0057 | 0.979700 |
| Resolution range (Å) | 50–1.5 | 50–1.4 |
| Last shell (Å) | 1.55–1.50 | 1.45–1.40 |
| $R_{sym}$ | 0.074 | 0.056 |
| Last shell | 0.344 | 0.503 |
| Completeness | 95.8 | 98.4 |
| Last shell | 81.9 | 85.9 |
| No. of reflections | 529,534 | 608,259 |
| Unique reflections | 158,345 | 103,337 |

TABLE IV
*Refinement and overall crystal structure statistics*

| Used data set | Native |
|---|---|
| Resolution range (Å) | 50.0–1.4 |
| *R*-factor ($R_{free}$) (%) | 13.3 (17.2) |
| No. of non-hydrogen protein atoms | 4443 |
| No. of water molecules | 665 |
| Average *B*-factor for chain A (B) (Å$^2$) | |
| Main chain atoms | 11.4 (12.8) |
| Side chain atoms | 14.3 (15.8) |
| Water molecules | 25.5 |
| Metal ions | 10.7 |
| Substrate molecules | 16.1 |
| r.m.s. deviation bond length (Å) | 0.023 |
| r.m.s. deviation bond angle (degrees) | 1.890 |
| Ramachandran plot | |
| Residues in most favorable regions (%) | 89.5 |
| Residues in additional regions (%) | 10.1 |
| Residues in disallowed regions (%) | 0.0 |

of peptidases from the MH clan: CPG2, PepT, PepV, AAP, and SGAP.[4] Models of the compared proteins were fitted, and r.m.s. calculations for C-$\alpha$ atoms were carried out using the Swiss-PDBviewer (41). For some secondary structure elements, additional local fitting was performed manually.

Figs. 1, 2, and 3*B* were made with Raster3D (available on the World Wide Web at www.bmsc.washington.edu/raster3d) (42).

## RESULTS AND DISCUSSION

*Structure of the Zinc-binding Domain in hAcy1*—During crystallization screening of different mutants of hAcy1, which are under investigation in our laboratory, only the T347G mutant gave crystals. Degradation of an intervening sequence, from residue 199 to 320, corresponding to the dimerization domain was observed, and only the large zinc-binding domain remained. The degradation occurred only after the protein was concentrated to 5–8 mg/ml for the crystallization trials. The intact T347G mutant only showed a 6.5-fold increase in $[S]_{0.5}$ and a reduction of $T_m$ by 7 °C (Table V), indicating that the mutation did not affect the catalytic machinery.

The crystal structure shows two molecules in the asymmetric unit with residues 7–198 and 321–408 well defined in molecule A (Fig. 1) and residues 8–197 and 321–405 in molecule B. The remaining domain adopts a typical carboxypeptidase A fold (43). It consists of an eight-stranded mixed $\beta$-sheet, flanked by three short $\alpha$-helices on one side and five long $\alpha$-helices on the other side. The model also contains 665 water molecules in the asymmetric unit and two zinc ions per molecule. The model shows good overall quality (see "Experimental Procedures"). The two molecules in the asymmetric unit are virtually identical and superimpose with a r.m.s. deviation of 0.33 Å for 273 C-$\alpha$ atoms. In the following, we only refer to molecule A.

$His^{80}$, $Asp^{113}$, $Glu^{148}$, $Glu^{175}$, and $His^{373}$ define a dinuclear zinc-binding site per molecule (Fig. 2). Each zinc ion is bound in pentadentate coordination to the side chains of a histidine, a glutamate, and a bridging aspartate residue. Furthermore, an additional small ligand molecule bridges the two zinc ions. Since the crystallization drop contained 10 mM L-norleucine, we interpreted the electron density of the ligand as a norleucine with a disordered side chain and modeled it as a glycine (Fig. 1).

*Zinc Centers in the Acy1/M20 and M28 Families*—The overall structure of the zinc-binding domain in the T347G mutant of hAcy1 (Fig. 1) is similar to the structures of the corresponding domains in the related enzymes CPG2, *S. typhimurium* PepT, and *L. delbrueckii* PepV as well as of the two single-domain enzymes AAP and SGAP from the M28 family. There are between 130 and 190 residues (of 280 residues) in our structure that superimpose with each of these domains with an r.m.s. deviation for C-$\alpha$ atoms of less than 1.8 Å. Sequence identities with hAcy1 for these protein domains range from 14.3% for AAP to 19.6% for CPG2. Below, we refer to the zinc ion furthest away from the central $\beta$-sheet in the MH clan peptidases as zinc 1 and to the other one as zinc 2.

The crystal structures of PepV, AAP, and SGAP were solved in complex with substrate analogs or products. In those complexes, the ligand occupies the same position as the modeled glycine in our aminoacylase structure (Fig. 2). In all cases, one of the carboxyl oxygen atoms (or an equivalent atom) occupies the bridging position between the two zinc ions, and the other oxygen coordinates zinc 1. $Glu^{147}$ in hAcy1, which serves as the putative general base, also occupies the same position in all structures compared here. One of the zinc ligands in the structural superposition is not fully conserved. The zinc 2-binding $Glu^{175}$ in hAcy1 and the equivalent glutamate in CPG2 are substituted by an aspartic acid in PepT, PepV, AAP, and SGAP (Fig. 2). It is noteworthy that an insertion before this zinc ligand of a phenylalanine in CPG2 and SGAP, a leucine in AAP, and a proline in PepV leads to local main chain adjustments in these enzymes compared with hAcy1 (not shown).

[4] The atomic coordinates for the crystal structures of CPG2, PepT, PepV, AAP, and SGAP are available in the Protein Data Bank (http://www.rcsb.org/pdb) under PDB numbers 1CG2, 1FNO, 1LFW, 1AMP, and 1QQ9, respectively (40).

TABLE V
*Kinetic parameters for the hydrolysis of $N^{\alpha}$-acetyl-L-methionine and stability parameters of wild-type and mutant hAcy1 enzymes*

| hAcy1 variant | $k_{cat}$ | $[S]_{0.5}$ | Hill coefficient ($n$) | $\Delta G(H_2O)$ | $T_m$ |
|---|---|---|---|---|---|
| | $s^{-1}$ | mM | | $kJ \cdot mol^{-1}$ | °C |
| Wild type | 38.3 ± 0.8 | 0.43 ± 0.03 | 1.16 ± 0.07 | 18.7 ± 0.10 | 64 |
| T347G | 46.0 ± 0.77 | 2.78 ± 0.11 | 1.28 ± 0.04 | ND[a] | 57 |
| E147A[b] | (10 ± 0.3)·$10^{-3}$ | 1.06 ± 0.11 | 1 | 18.0 ± 0.50 | 61 |
| E147Q[b] | (4.43 ± 0.11)·$10^{-3}$ | 0.71 ± 0.06 | 1 | 13.2 ± 0.10 | 64 |
| E147D | NM[c] | | | NM | NM |
| H80A (Zn2)[b] | (15.89 ± 0.75)·$10^{-3}$ | 2.02 ± 0.30 | 1 | 14.8 ± 0.24 | 45 |
| D113A (Zn1/2)[b] | (2.19 ± 0.01)·$10^{-3}$ | 0.57 ± 0.10 | 1 | 8.3 ± 0.04 | 46 |
| E148A (Zn1)[b] | (52.5 ± 3.9)·$10^{-3}$ | 2.96 ± 0.05 | 1 | 11.5 ± 0.10 | 46 |
| E175A (Zn2) | (0.84 ± 0.02)·$10^{-3}$ | 0.71 ± 0.05 | 1.16 ± 0.08 | 14.9 ± 0.10 | 47 |
| H373A (Zn1)[b] | (1.35 ± 0.1)·$10^{-3}$ | 2.82 ± 0.30 | 1 | 16.0 ± 0.20 | 50 |
| H206N[b] | (15.2 ± 0.4)·$10^{-3}$ | 2.02 ± 0.15 | 1 | 16.8 ± 0.20 | 54 |
| H206N/E147Q | 10.26 ± 0.35 | 0.74 ± 0.06 | 1.13 ± 0.05 | ND | 58 |
| H206N/E147D | 2.18 ± 0.01 | 0.72 ± 0.04 | 1.06 ± 0.04 | ND | 33 |
| H206N/D113A | 5.79 ± 0.19 | 0.91 ± 0.07 | 1.07 ± 0.04 | ND | 45 |

[a] ND, not determined.
[b] No cooperativity was observed, and $[S]_{0.5} = K_M$ and $n = 1$.
[c] NM, not measurable.

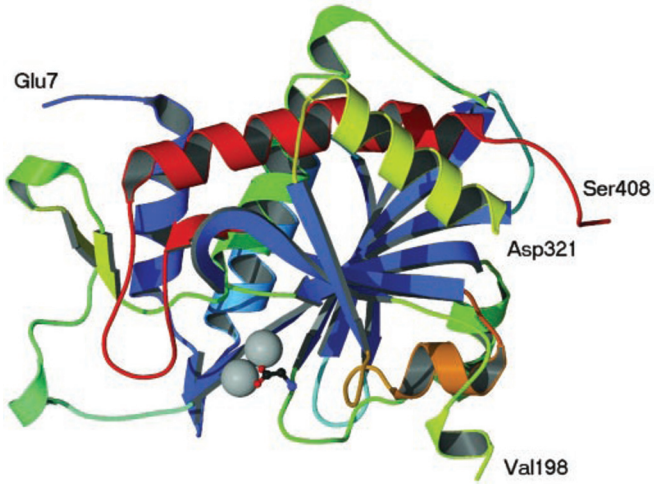


FIG. 1. **Ribbon diagram of the zinc-binding domain in the T347G mutant of hAcy1.** Glycine was modeled in place of a putative L-norleucine ligand molecule and is shown in a *ball-and-stick* representation. Zinc ions are represented as *gray spheres*.

Nevertheless, the zinc-zinc and most of the zinc-ligand distances in the dinuclear centers are similar among the compared structures (Table VI). The zinc 1-ligand distances in PepT, however, are 0.3–0.8 Å longer than in the other enzymes. This suggests that zinc 1 in PepT may show higher Lewis acidity.

An analysis of the Acy1/M20 sequence family revealed that all homologs with proven aminopeptidase or dipeptidase specificity, including PepT, PepV, X-His dipeptidase, and mammalian nonspecific dipeptidase and carnosinase (15, 17, 44) (Table I), contain an aspartic acid in this zinc ligand position. On the other hand, Acy1/M20 family members that exhibit either aminoacylase or carboxypeptidase specificity, such as Acy1, *N*-acetylornithine deacetylase, and succinyldiaminopimelate desuccinylase enzymes or CPG2 and *S. cerevisiae* carboxypeptidase Y (Table I), have a glutamic acid residue in the same position (5). Remarkably, to the best of our knowledge, no genuine carboxypeptidase activity for CPG2 has been reported. CPG2 was originally identified as a folate hydrolase (9, 11). In addition, the enzyme was shown to display dipeptidase specificity, with a requirement for glutamate in the carboxyl-terminal position (10). Since glutamate was also liberated from an N-terminally blocked dipeptide, benzyloxycarbonyl-glycyl-glutamate, the trivial name carboxypeptidase G was proposed.

In the PepV crystal structure, zinc 2 and the nonconserved zinc 2 ligand, $Asp^{177}$, were suggested to be involved in substrate binding (29). In the structure of this enzyme, the free amino group of the bound inhibitor, Asp$\Psi$[$PO_2CH_2$]AlaOH, is interacting with zinc 2 and the main chain oxygen of its ligand $Asp^{177}$. In hAcy1 and CPG2, however, the longer glutamic acid side chain at this position accounts for a ~3 Å longer distance between zinc 2 and the respective main chain oxygen atom compared with both PepV and PepT (Table VI). This would probably not allow the simultaneous docking of a free substrate amino group by zinc 2 and the respective ligand main chain oxygen in these enzymes. In view of that, CPG2 and hAcy1 accommodate acyl moieties of varied size in their $S_1$ pockets (11, 45) instead of terminal amino acid residues as PepV and PepT do. In the M28 family, no similar correlation between zinc 2 ligation and specificity can be observed as judged by the sequence alignment at the MEROPS data base (available on the World Wide Web at merops.sanger.ac.uk). An aspartic acid serves as a zinc 2 ligand, for instance, in the two genuine aminopeptidases AAP and SGAP and also in human glutamate carboxypeptidase II, also known as prostate-specific membrane antigen (46).

*Characterization of hAcy1 Mutants*—All mutants of hAcy1 generated during this work (see Table II) showed the same expression and purification behavior as reported for the wild-type enzyme (30). They also revealed the same electrophoretic mobility as the wild-type enzyme in SDS and native polyacrylamide gels (not shown). Effects of the mutations on protein stability and catalytic activity were investigated. The stabilization energy, $\Delta G(H_2O)$, was determined by recording the loss of cumulative tryptophan fluorescence after equilibrium denaturation with guanidine hydrochloride and therefore represents the overall protein stability (Table V). The "melting temperature," $T_m$, was determined by monitoring enzymatic activity and therefore reflects loss of active site integrity (Table V). The transition curves obtained during the stability measurements indicate a folded state for all but one of the mutant enzymes. The E147D mutant became increasingly unstable at low denaturant concentrations so that $\Delta G(H_2O)$ could not be determined quantitatively.

Kinetic measurements were performed using $N^{\alpha}$-acetyl-L-methionine as enzyme substrate (Table V). The same relative values for kinetic parameters were obtained with $N^{\alpha}$-formyl-L-norleucine as the substrate (not shown). All mutations discussed below resulted in a reduction of the catalytic constant, $k_{cat}$, by 3–4 orders of magnitude. No activity could be detected for the E147D mutant. The substrate concentration at half-saturation, which throughout is given by the $[S]_{0.5}$ or $K_m$ values

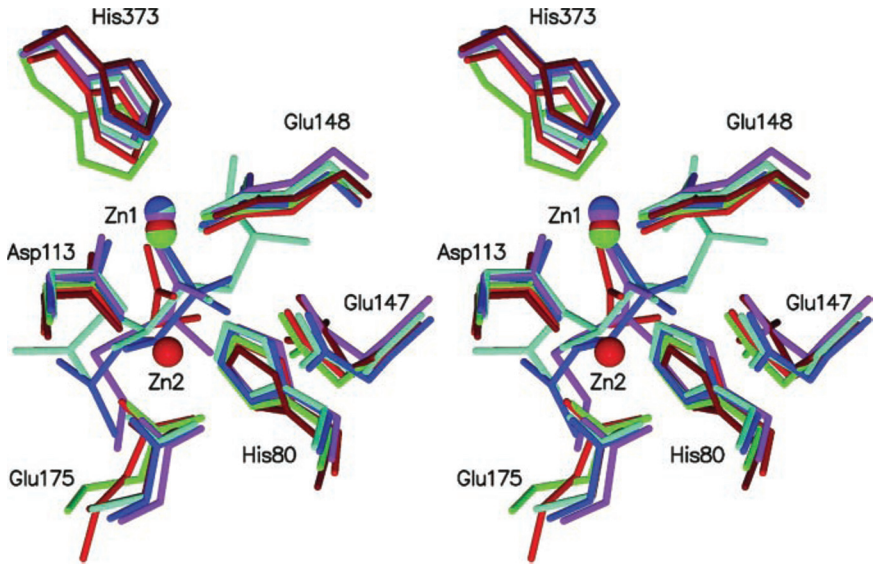


FIG. 2. **Stereo close-up view of the superposition of the zinc centers in the T347G mutant of hAcy1 in complex with glycine, *Pseudomonas* sp. CPG2 and *S. typhimurium* PepT (both without ligand), and *L. delbrueckii* PepV, AAP, and SGAP in complex with AspΨ[$PO_2CH_2$]AlaOH, L-leucinephosphonic acid and methionine, respectively.** The structures are colored in *red*, *green*, *brown*, *cyan*, *blue*, and *purple* for hAcy1, CPG2, PepT, PepV, AAP, and SGAP, respectively. Only amino acid side chains are shown. The numbering is given for hAcy1. During the superposition, zinc 2 was taken as the first and the zinc 1 as the second fixed point, followed by alignment with the C-γ atom of $Asp^{113}$.

TABLE VI
*Protein-metal distances in angstroms in the crystal structures of hAcy1 (T347G mutant), Pseudomonas sp. CPG2, S. typhimurium PepT, L. delbrueckii PepV, AAP, and SGAP*

Residue numbers are given for hAcy1.

| | Zn–Zn | $His^{373}$–Zn1 | $Asp^{113}$–Zn1 | $Glu^{148}$ O-1–Zn1 | $Glu^{148}$ O-2–Zn1 | $His^{80}$–Zn2 | $Asp^{113}$–Zn2 | $Glu^{175a}$ O-1–Zn2 | $Glu^{175a}$ O-2–Zn2 | $Glu^{175a}$ main chain O–Zn2 |
|---|---|---|---|---|---|---|---|---|---|---|
| hAcy1 | 3.36 | 2.03 | 2.01 | 2.00 | 2.40 | 2.02 | 2.00 | 1.96 | 2.52 | 7.24 |
| CPG2 | 3.25 | 1.98 | 2.03 | 2.09 | 2.48 | 2.07 | 1.96 | 1.97 | 2.45 | 7.28 |
| PepT | 3.38 | 2.69 | 2.32 | 2.49 | 3.20 | 2.22 | 1.98 | 2.18 | 2.53 | 4.53 |
| PepV | 3.84 | 1.94 | 1.90 | 1.92 | 2.56 | 2.06 | 2.04 | 2.10 | 2.30 | 4.13 |
| AAP | 3.47 | 2.32 | 2.05 | 2.04 | 2.38 | 2.21 | 2.01 | 2.05 | 2.34 | 5.35 |
| SGAP | 3.80 | 2.05 | 1.99 | 2.02 | 2.66 | 1.96 | 2.07 | 2.00 | 2.81 | 5.26 |

[a] HAcy1 and CPG2 have a glutamate in this position, whereas PepT, PepV, AAP, and SGAP have an aspartate.

obtained by the Hill or Michaelis-Menten equation (see "Experimental Procedures"), respectively, increased up to 7-fold for the T347G, H80A, E148A, H373A, and H206N mutants. Compared with the above-mentioned changes in $k_{cat}$, these differences are much lower, and their significance is less clear.

*The Zinc Center and $Glu^{147}$ in hAcy1*—Attempts to determine metal-binding stoichiometries in enzymes of the Acy1/M20 family by spectroscopic methods frequently showed only one zinc atom per monomer (27, 27, 47, 48). Moreover, in the crystal structure of PepT, the occupancy of the zinc 1 site was low (24), which may indicate a low affinity zinc-binding site. On the contrary, in AAP zinc 1 appears to be bound stronger than zinc 2, and the enzyme exhibits 80% of its catalytic activity with zinc 1 alone (49). In order to assess the importance of both metal-binding sites in the dinuclear zinc center of hAcy1, we mutated individually each of the five zinc-binding residues to alanine (H80A, D113A, E148A, E175A, and H373A). These mutations resulted in $10^3$- to $10^4$-fold catalytic inactivations (Table V). No trends were observed in the half-saturation substrate concentrations and $\Delta G(H_2O)$ values by mutations of zinc 1 or zinc 2 ligands, respectively. Mutation of the zinc-bridging residue $Asp^{113}$ (Fig. 2), however, clearly led to the highest loss in overall stability among the five mutants. The results indicate that both zinc sites are essential for catalysis and suggest that only a fully intact zinc center confers optimal enzyme stability.

A conserved glutamic acid residue, $Glu^{147}$ in hAcy1, in the immediate vicinity of the zinc center (Fig. 2) in the MH clan is thought to act as a general base during catalysis, accepting a proton from the zinc-bound water molecule. Replacing $Glu^{147}$ with an alanine (E147A) or glutamine (E147Q) led to a 1000-fold decrease in enzyme activity. No activity was detectable, and no stability data could be obtained with the aspartate mutant (E147D). To understand this pronounced effect of the Glu-to-Asp mutation, we modeled this replacement in the structure of hAcy1 (not shown). Shortening the amino acid side chain in this position not only brings its acidic group away from the appropriate position for activation of the catalytic water molecule but also positions it closer to $Asp^{348}$, possibly introducing an unfavorable interaction between the two residues.

*Two Subdomains in the Lid Domain of PepV Mimic a Dimer*—In contrast to the single-domain enzymes from the M28 family, Acy1/M20 family enzymes generally contain a second, smaller domain, the possible role of which in catalysis is not clear. As mentioned above, most of these enzymes exist as homodimers. In CPG2 and *S. typhimurium* PepT, the small domains were shown to mediate enzyme dimerization through side-by-side packing of their four-stranded β-sheets, thereby forming a contiguous extended eight-stranded sheet (23, 24). In contrast, *L. delbrueckii* PepV exists in a monomeric form (29). The crystal structure of this enzyme revealed that its small domain contains a central eight-stranded β-sheet. Here, we recognize that this domain can be subdivided into two subdomains, each composed of six β-strands. Subdomain 1 encompasses strands 1, 8, 9, 10, 11, and 12 and helices III and IV, whereas subdomain 2 includes strands 2, 3, 4, 5, 6, and 7 and

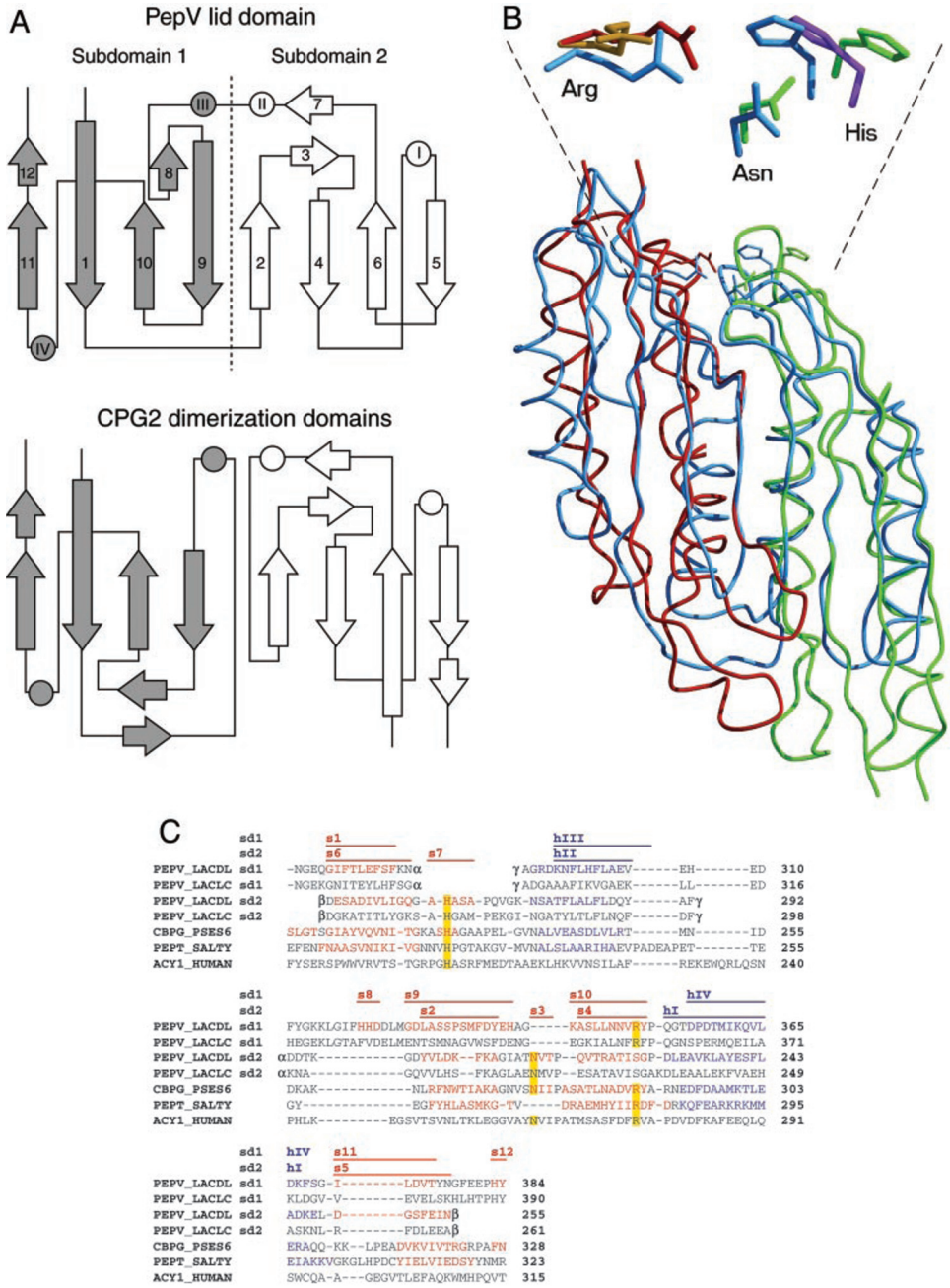


FIG. 3. **Structures of the small domains of enzymes from the Acy1/M20 family.** *A*, topology diagram for the lid domain in *L. delbrueckii* PepV and the dimerization domains from both monomers in *Pseudomonas* sp. CPG2. Subdomains 1 (*gray*) and 2 (*white*) of PepV show apparent similarity. However, strands 8 and 12 are only found in subdomain 1, and strands 3 and 7 are only found in subdomain 2. The $\beta$-sheet composed of the latter two strands is also present in the dimerization domain of CPG2. *B*, backbone trace superposition of subdomains 1 and 2 in the lid domain of PepV (*blue*) and the two associated dimerization domains in CPG2 (*red* and *green*). Known active site residues in PepV are shown in a *stick* representation, from *left* to *right*, $Arg^{350}$, $Asn^{217}$ (both carboxyl-terminal docking), and $His^{269}$ (transition state stabilization). Corresponding residues from CPG2 are also shown. The *enlargement above* additionally shows the corresponding residues in PepT. $Arg^{288}$ from CPG2 (*red*) and $Arg^{280}$ from PepT (*yellow*) reside in the monomer, which superimposes with subdomain 1 of PepV. $Asn^{275}$ and $His^{229}$ from CPG2 (*green*) and $His^{223}$ in PepT (*purple*) are recruited from the opposite monomer which superimposes with subdomain 2 of PepV. In the structure of CPG2, the side chain of $His^{229}$ shows a $\chi_1$ rotation by about 90° relative to the other two structures and coordinates an additional interdimeric zinc ion in the protein crystal (not shown). *C*, multiple sequence alignment of the small domains in the PepV enzymes from *L. delbrueckii* (PEPV_LACDL) and *Lactococcus lactis* subsp. *cremoris* MG1363 (PEPV_LACLC) and from CPG2 (CBPG_PSES6), PepT (PEPT_SALTY), and hAcy1 (ACY1_HUMAN). Subdomain 1 and 2 in the lid domain of PepV are abbreviated sd1 and sd2, respectively. The alignment was assembled using an available alignment of the two PepV enzymes (15) and structure-based alignments of CPG2 to sd1 in *L. Delbrueckii* (29) and CPG2 to PepT (24). The sequences of the dimerization domain in hAcy1 and CPG2 were aligned manually. Strands (*s*) and helices (*h*), as identified in the crystal structures of PepV, CPG2, and PepT, are printed in *red* and *blue*, respectively. Their numbering in sd1 and sd2 of *L. delbrueckii* PepV is indicated in the corresponding *colors above* the aligned sequences. Residues that interact with the bound transition state analog $Asp\Psi[PO_2CH_2]AlaOH$ in the PepV structure are in *yellow boxes*. *Greek letters* indicate the sites of rearrangement generated by the insertion of sd2 in the sequence of sd1 and their sequel.

helices I and II (Fig. 3). Whereas the resemblance of subdomain 1 to the dimerization domain of CPG2 was previously noted (29), we extend this observation by recognition that subdomain 2 also has the same topology as the dimerization domain of CPG2 (Fig. 3*A*) and of PepT (not shown). More importantly, we demonstrate that the two subdomains in the lid domain of

PepV mimic the arrangement of the two dimerization domains within the CPG2 and PepT dimers. The superposition of the entire small domain of PepV on the small domains of the CPG2 dimer (Fig. 3*B*) overlaps 196 C-$\alpha$ atoms of 230 with an r.m.s. deviation of 1.54 Å. In PepT, 208 C-$\alpha$ atoms out of 230 accordingly superimpose with an r.m.s. deviation of 1.62 Å. Two of three residues from the PepV lid domain, which interact with the bound transition state analog Asp$\Psi$[$PO_2CH_2$]AlaOH (29) (*i.e.* His$^{269}$ in subdomain 2 and Arg$^{350}$ in subdomain 1 of PepV) are also found in the dimerization domains of CPG2, PepT (Fig. 3*B*), and, by a multiple sequence alignment of small domains from the Acy1/M20 family, also in hAcy1 (Fig. 3*C*). The third residue, Asn$^{217}$ in subdomain 2, is missing only in PepT. His$^{269}$ was assigned a role in transition state stabilization, and Arg$^{350}$ and Asn$^{217}$ were assigned roles in anchoring the free C terminus of the substrate (29). At the time of writing, these three residues were found to be conserved in 98, 89, and 72% of Acy1/M20 family sequences, respectively (available on the World Wide Web at merops.sanger.ac.uk/). Beyond that, there is no identifiable sequence identity between subdomains 1 and 2 in PepV and any of the dimerization domains compared here (Fig. 3*C*), which reinforces the functional significance of the histidine, arginine, and, possibly, asparagine conservations.

Recently, Sintchak *et al.* (50) reported the case of a monomeric enzyme that is reminiscent of PepV. The crystal structure of class II ribonucleotide triphosphate reductase from *Lactobacillus leichmannii* revealed that a 130-amino acid insertion in the core $\alpha/\beta$-barrel of the monomeric enzyme mimics a dimer. In the structures of related dimeric class I ribonucleotide reductases, each of the two subunits contributes one-half of a four-helix bundle, on top of which an allosteric effector-binding region is located. In the monomeric class II ribonucleotide triphosphate reductase, the 130-amino acid insertion provides the second half of this four-helix bundle. Thereby, allosteric control of substrate specificity in the monomer occurs, presumably, by the same mechanism as in the dimeric enzymes.

*Catalysis in hAcy1 Occurs at the Dimer Interface*—We also investigated the role of a conserved histidine in the small domain of the Acy1/M20 family of enzymes (5). The respective His$^{269}$ from the lid domain of *L. delbrueckii* PepV functions in the stabilization of the transition state (29). This residue corresponds to His$^{229}$, His$^{223}$, and His$^{206}$ in the small domains of the dimeric homologs CPG2, PepT, and hAcy1, respectively (Fig. 3*C*). In the crystal structures of CPG2 and PepT, the two enzyme domains appear to be connected by flexible linkers and show an open conformation. In both structures, the histidine is solvent-exposed and is located 50 Å from the metal center in the same monomer and more than 8 Å from the metal center in the opposite monomer of the dimer. His$^{229}$ in CPG2 coordinates an additional interdimeric zinc ion, which is further coordinated by Asp$^{387}$ from another dimer within the crystallographic tetramer. His$^{223}$ in PepT contributes to the binding of a putative sulfate ion in the crystal structure, which was suggested to occupy a binding site for the C-terminal carboxyl group of the tripeptide substrate (24). On the basis of these observations, His$^{206}$ in hAcy1 was selected for mutation. A His-to-Asn mutation generated an enzyme with a 2000-fold decrease in $k_{cat}$ and a 10 °C reduced $T_m$ value (Table V). These effects on activity and $T_m$ are largely comparable with those observed upon mutation of any of the zinc-binding residues.

The detrimental effect on activity by the His-to-Asn mutation in position 206 of hAcy1, and the structural resemblance between the lid domain of PepV and the two associated dimerization domains in CPG2 (Fig. 3), discussed above, led us to hypothesize that the conserved histidine in the dimerization

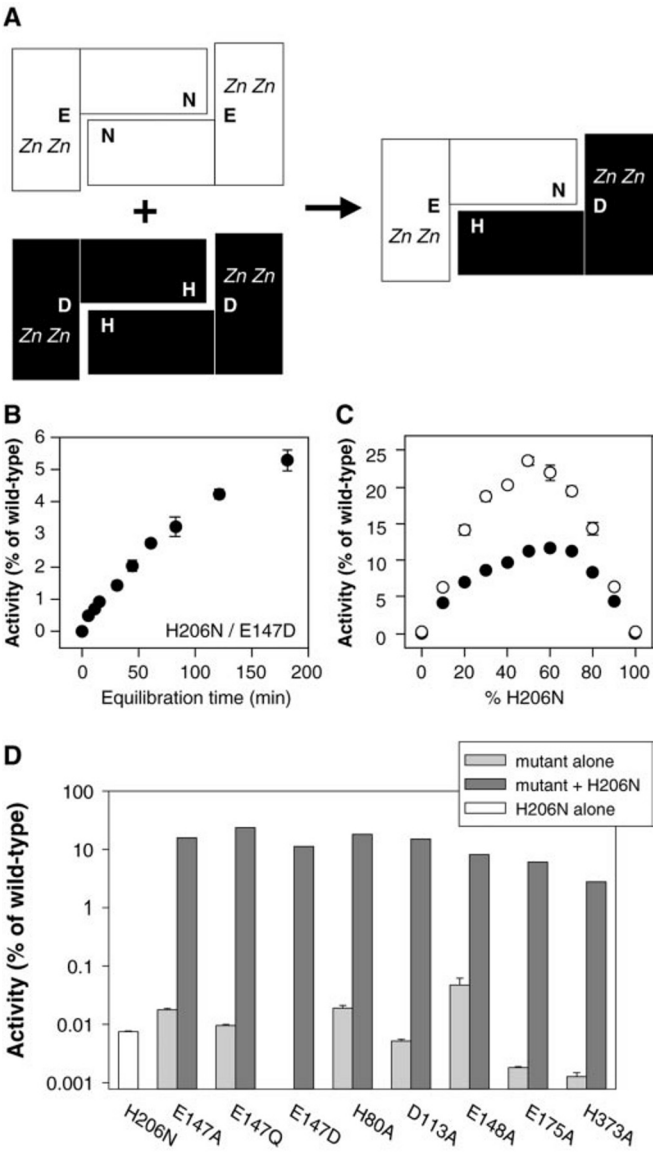


FIG. 4. **Enzyme complementation assay.** *A*, schematic representation of heterodimer formation between the H206N (*white*) and E147D (*black*) mutants of hAcy1. *Zn Zn* indicates the dinuclear zinc center. *H* and *E* represent His$^{206}$ and Glu$^{147}$, respectively. Accordingly, *N* and *D* indicate the asparagine and aspartic acid mutations in these two positions. H206N was mixed with mutants of the zinc-binding domain of hAcy1 to yield total protein concentrations of 150 $\mu$g/ml. After an equilibration period, samples were assayed for *N*-acetyl-L-methionine (10 mM)-hydrolyzing activity for 20 min. *B*, time dependence of activity reappearance after mixing of H206N and E147D in equal amounts. *C*, recovered activity after 16 h with varying ratios of H206N/E147D (●) and H206N/E147Q (○). *D*, recovered activity after 16 h at 1:1 ratios of H206N to each of the zinc-binding domain mutants.

domain of dimeric Acy1/M20 family enzymes contributes *in trans* to the active site. In order to test directly this hypothesis, we took advantage of the existence of two separate active sites within the dimer to design an enzyme complementation assay. Mixing two different mutants should lead upon equilibration to the formation of heterodimers. If two inactivating mutations act *in trans*, one catalytic site in these heterodimers harbors both mutations, whereas the other is functional (Fig. 4*A*). When equimolar amounts of the two mutants H206N and E147D were mixed together, a partial recovery of catalytic activity over time was observed, amounting to 11% of the wild-type activity (Fig. 4*B*). Similar recovery of activity was observed for the combination of H206N with E147Q. Variations

of the H206N/E147D and H206N/E147Q ratios yielded activity optima at approximately equimolar ratios (Fig. 4*C*), indicating that homo- and heterodimers formed with equal affinities and that the mutations did not interfere with dimerization itself. Equilibration of the H206N mutant with each of the metal-binding domain mutants at 1:1 ratios also led to recovery of catalytic activity, which reached between 3% (H206N/H373A) and 24% (H206N/E147Q) of the wild-type activity (Fig. 4*D*). This is in the range of the calculated maximum theoretical value of 16.7% wild-type activity (Table V), which would be expected when the solution contains equal amounts of all three dimeric species, and when there is no interdependence between the two active sites in the dimer. Accordingly, similar half-saturation substrate concentrations as in the wild type for three selected heterodimer combinations, H206N with E147D, E147Q, and D113A, indicate unchanged substrate affinities. Notably, the complementation assay also showed that inactivation of the E147D mutant was not associated with irreversible unfolding of this protein. The active site stabilities in the three combinations, as measured by $T_m$, follow the order of the $\Delta G(H_2O)$ values for the three mutants E147D, E147Q, and D113A alone (Table VI). This probably reflects the impact of each of these mutations on the overall stability of the respective heterodimer with the H206N mutant.

*A Revised Catalytic Site in the Acy1/M20 Family*—The M28 family enzymes AAP and SGAP are believed to follow a zinc peptidase mechanism, which requires both metal ions for full activity (21, 51). This mechanism is assumed to be operational in all enzymes from the MH clan, which are therefore called co-catalytic metallopeptidases (2, 14). In support of this conclusion, the dinuclear zinc center and the putative general base residue, $Glu^{147}$ in hAcy1, and in six available structures from the MH clan superimpose well (Fig. 2). Furthermore, the results from our mutational analysis of hAcy1 from the Acy1/M20 family corroborate the catalytic significance of a fully intact dizinc center and $Glu^{147}$. Previous nuclear magnetic relaxation studies of manganese-substituted porcine Acy1 in complex with *t*-butoxycarbonyl amino acid inhibitors indicated metal-inhibitor distances of at least 12 Å, which suggested not a catalytic but a purely structural role for the zinc center (52). We speculate that the binding of these competitive inhibitors to porcine Acy1 may not, however, be representative of catalytically competent enzyme-substrate complexes.

Previously, Wouters and Husain (2) argued that, among the co-catalytic exopeptidases, neither amino- nor carboxyl-terminal docking of the substrate would restrict peptidase phenotypes, because corresponding docking groups among these enzymes were found not to be conserved. However, among the known enzymes of the Acy1/M20 family (Table I), the presence of an aspartate as zinc 2 ligand is associated with aminopeptidase or dipeptidase rather than aminoacylase or carboxypeptidase specificities. It remains to be shown whether this feature generally contributes to substrate specificity in this enzyme family, as suggested for the dipeptidase PepV (29). In hAcy1, the Glu-to-Asp mutation in the corresponding position 175 led to an over 1000-fold loss in enzyme activity in our standard aminoacylase assay and did not convert the enzyme into a dipeptidase. Neither wild type nor mutant showed detectable activity against L-leucyl-L-alanine, L-alanyl-L-leucine, or L-leucyl-glycine. It appears that additional farther ranging adjustments in protein structure contribute to the peptidase phenotype.

A specific finding from this study is the importance for enzyme activity of the conserved $His^{206}$ from the small domain in hAcy1. $His^{206}$ aligns with $His^{269}$ in the lid domain of PepV (Fig. 3*C*), which together with zinc 1 forms an oxyanion-binding hole for the stabilization of the tetrahedral intermediate (29). In the single-domain enzyme SGAP, $Tyr^{246}$, which resides in an extended loop over the active site, and zinc 1 are believed to function in a similar way (22). In our structure superposition of zinc-binding domains, the ligand-hydrogen bonds formed by $Tyr^{246}$ in SGAP and $His^{269}$ in PepV (not shown) are equivalent, accordingly. Although we also found tyrosines in the zinc-binding domains of CPG2 and PepT in similar positions as $Tyr^{246}$ in SGAP, (*i.e.* $Tyr^{384}$ and $Tyr^{378}$, respectively), they exhibit very different side chain conformations and could not be superimposed with $Tyr^{246}$. Conclusively, the conserved histidine in the small domain of Acy1/M20 family enzymes may play a similar role as $Tyr^{246}$ in SGAP. The results from the complementation assay (Fig. 4) indicate that in dimeric hAcy1 this histidine is acting *in trans*.

The open conformation in the crystal structures of CPG2 and PepT most likely does not present catalytically competent enzymes. Based on the results from our structural and mutational analyses, we put forward the following hypothesis to explain active site formation in dimeric enzymes of the Acy1/M20 family. A conformational change, possibly induced by substrate binding, brings two residues in the dimerization domain, a conserved histidine ($His^{206}$ in hAcy1) and an asparagine ($Asn^{263}$ in hAcy1), in the vicinity of the zinc center from the opposite monomer. Concomitantly, a highly conserved arginine ($Arg^{276}$ in hAcy1) from the dimerization domain in the same monomer as the zinc center may be inserted in the active site. Whereas our data from hAcy1 support a catalytic role for the histidine residue, proposed roles of the arginine and asparagine residues in carboxyl-terminal docking of the substrate, similar to PepV (29), remain to be tested. The lack of this asparagine in PepT (Fig. 3*B*) could be related to this enzyme being an amino tripeptidase, accommodating a longer substrate.

This study may inspire strategies for the improvement of Acy1/M20 family enzymes toward applications in biocatalysis or cancer therapy. In ADEPT, a tumor-targeted version of CPG2 is currently used to convert a prodrug to a cytotoxic agent. However, the first clinical trials demonstrated a strong immune response to the bacterial enzyme, a major obstacle to its use as a cancer therapeutic (53). The first structure of a human homolog, hAcy1, provides a rational foundation for the silencing of immunogenic sites in the zinc-binding domain of CPG2 (54) by humanization or for the engineering of the specificity of the human enzyme to perform the same function as CPG2 in ADEPT.

*Acknowledgments*—We are indebted to Dr. Klaus-Heinrich Röhm for generously providing the baculovirus transfer vector pVL1393-hAcI. We thank Dr. Traian Sulea for the sequence alignment of the dimerization domains of CPG2 and hAcy1 and Lorena Boju and Dr. Jayaraman Sivaraman for technical assistance. We thank Dr. Florence Fassy for critical reading of the manuscript.

REFERENCES

1. Holz, R. C., Bzymek, K. P., and Swierczek, S. I. (2003) *Curr. Opin. Chem. Biol.* **7,** 197–206
2. Wouters, M. A., and Husain, A. (2001) *J. Mol. Biol.* **314,** 1191–1207
3. Rawlings, N. D., O'Brien, E., and Barrett, A. J. (2002) *Nucleic Acids Res.* **30,** 343–346
4. Schmiedeberg, O. (1881) *Naunym-Schmiedberg's Arch. Exp. Pathol. Pharmakol.* **14,** 379–392
5. Biagini, A., and Puigserver, A. (2001) *Comp. Biochem. Physiol. B Biochem. Mol. Biol.* **128,** 469–481
6. Gade, W., and Brown, J. L. (1981) *Biochim. Biophys. Acta* **662,** 86–93
7. Jones, W. M., Scaloni, A., Bossa, F., Popowicz, A. M., Schneewind, O., and Manning, J. M. (1991) *Proc. Natl. Acad. Sci. U. S. A.* **88,** 2194–2198
8. Boyen, A., Charlier, D., Charlier, J., Sakanyan, V., Mett, I., and Glansdorff, N. (1992) *Gene* (*Amst.*) **116,** 1–6
9. Levy, C. C., and Goldman, P. (1967) *J. Biol. Chem.* **242,** 2933–2938
10. Goldman, P., and Levy, C. C. (1967) *Proc. Natl. Acad. Sci. U. S. A.* **58,** 1299–1306
11. Sherwood, R. F., Melton, R. G., Alwan, S. M., and Hughes, P. (1985) *Eur. J. Biochem.* **148,** 447–453

12. Spormann, D. O., Heim, J., and Wolf, D. H. (1992) *J. Biol. Chem.* **267,** 8021–8029
13. Vongerichten, K. F., Klein, J. R., Matern, H., and Plapp, R. (1994) *Microbiology* **140,** 2591–2600
14. Barrett, A. J., Rawlings, N. D., and Woessner, J. F. (1998) in *Handbook of Proteolytic Enzymes* (Barrett, A. J., Rawlings, N. D., and Woessner, J. F., eds) pp. 1412–1416, Academic Press, London
15. Hellendoorn, M. A., Franke-Fayard, B. M., Mierau, I., Venema, G., and Kok, J. (1997) *J. Bacteriol.* **179,** 3410–3415
16. Schroeder, U., Henrich, B., Fink, J., and Plapp, R. (1994) *FEMS Microbiol. Lett.* **123,** 153–159
17. Teufel, M., Saudek, V., Ledig, J. P., Bernhardt, A., Boularand, S., Carreau, A., Cairns, N. J., Carter, C., Cowley, D. J., Duverger, D., Ganzhorn, A. J., Guenet, C., Heintzelmann, B., Laucher, V., Sauvage, C., and Smirnova, T. (2003) *J. Biol. Chem.* **278,** 6521–6531
18. Kawasaki, S., Miyake, C., Kohchi, T., Fujii, S., Uchida, M., and Yokota, A. (2000) *Plant Cell Physiol.* **41,** 864–873
19. Bommarius, A. S. (2002) in *Enzyme Catalysis in Organic Synthesis* (Drauz, K., and Waldmann, H., eds) pp. 741–749, Wiley-VCH, Weinheim
20. Burke, P. J. (2000) *Expert Opin. Ther. Pat.* **10,** 209–214
21. Chevrier, B., Schalk, C., D'Orchymont, H., Rondeau, J. M., Moras, D., and Tarnus, C. (1994) *Structure* **2,** 283–291
22. Gilboa, R., Spungin-Bialik, A., Wohlfahrt, G., Schomburg, D., Blumberg, S., and Shoham, G. (2001) *Proteins* **44,** 490–504
23. Rowsell, S., Pauptit, R. A., Tucker, A. D., Melton, R. G., Blow, D. M., and Brick, P. (1997) *Structure* **5,** 337–347
24. Hakansson, K., and Miller, C. G. (2002) *Eur. J. Biochem.* **269,** 443–450
25. Palm, G. J., and Rohm, K. H. (1995) *J. Protein Chem.* **14,** 233–240
26. Lindner, H., Berens, W., Kraus, I., and Röhm, K. H. (2000) *Biol. Chem.* **381,** 1055–1061
27. Kördel, W., and Schneider, F. (1977) *Z. Naturforsch. C* **32,** 342–344
28. Bosman, B. W., Tan, P. S. T., and Konings, W. N. (1990) *Appl. Environ. Microbiol.* **56,** 1839–1843
29. Jozic, D., Bourenkow, G., Bartunik, H., Scholze, H., Dive, V., Henrich, B., Huber, R., Bode, W., and Maskos, K. (2002) *Structure* **10,** 1097–1106
30. Pittelkow, S., Lindner, H., and Röhm, K. H. (1998) *Protein Expression Purif.* **12,** 269–276
31. Bradford, M. M. (1976) *Anal. Biochem.* **72,** 248–254
32. Otwinowski, Z., and Minor, W. (1997) *Methods Enzymol.* **276,** 307–326
33. Terwilliger, T. C., and Berendzen, J. (1999) *Acta Crystallogr. Sect. D Biol. Crystallogr.* **55,** 849–861
34. Terwilliger, T. C. (2000) *Acta Crystallogr. Sect. D Biol. Crystallogr.* **56,** 965–972
35. Perrakis, A., Morris, R., and Lamzin, V. S. (1999) *Nat. Struct. Biol.* **6,** 458–463
36. Jones, T. A., Zou, J. Y., Cowan, S. W., and Kjeldgaard (1991) *Acta Crystallogr. Sect. A* **47,** 110–119
37. Murshudov, G. N., Vagin, A. A., and Dodson, E. J. (1997) *Acta Crystallogr. Sect. D Biol. Crystallogr.* **53,** 240–255
38. Brunger, A. T., Adams, P. D., Clore, G. M., DeLano, W. L., Gros, P., Grosse-Kunstleve, R. W., Jiang, J. S., Kuszewski, J., Nilges, M., Pannu, N. S., Read, R. J., Rice, L. M., Simonson, T., and Warren, G. L. (1998) *Acta Crystallogr. D Biol. Crystallogr.* **54,** 905–921
39. Laskowski, R. A., MacArthur, M. W., Moss, D. S., and Thornton, J. M. (1993) *J. Appl. Crystallogr.* **26,** 283–291
40. Berman, H. M., Westbrook, J., Feng, Z., Gilliland, G., Bhat, T. N., Weissig, H., Shindyalov, I. N., and Bourne, P. E. (2000) *Nucleic Acids Res.* **28,** 235–242
41. Guex, N., and Peitsch, M. C. (1997) *Electrophoresis* **18,** 2714–2723
42. Merritt, A., and Bacon, D. J. (1997) *Methods Enzymol.* **277,** 505–524
43. Rees, D. C., Lewis, M., and Lipscomb, W. N. (1983) *J. Mol. Biol.* **168,** 367–387
44. Schrögel, O., Krispin, O., and Allmansberger, R. (1996) *FEMS Microbiol. Lett.* **145,** 341–348
45. Chenault, H. K., Dahmer, J., and Whitesides, G. M. (1989) *J. Am. Chem. Soc.* **111,** 6354–6364
46. Rawlings, N. D., and Barrett, A. J. (1997) *Biochim. Biophys. Acta* **1339,** 247–252
47. Born, T. L., Zheng, R., and Blanchard, J. S. (1998) *Biochemistry* **37,** 10478–10487
48. Javid-Majd, F., and Blanchard, J. S. (2000) *Biochemistry* **39,** 1285–1293
49. Prescott, J. M., Wagner, F. W., Holmquist, B., and Vallee, B. L. (1983) *Biochem. Biophys. Res. Commun.* **114,** 646–652
50. Sintchak, M. D., Arjara, G., Kellogg, B. A., Stubbe, J., and Drennan, C. L. (2002) *Nat. Struct. Biol.* **9,** 293–300
51. Greenblatt, H. M., Almog, O., Maras, B., Spungin-Bialik, A., Barra, D., Blumberg, S., and Shoham, G. (1997) *J. Mol. Biol.* **265,** 620–636
52. Heese, D., Berger, S., and Röhm, K. H. (1990) *Eur. J. Biochem.* **188,** 175–180
53. Francis, R. J., Sharma, S. K., Springer, C., Green, A. J., Hope-Stone, L. D., Sena, L., Martin, J., Adamson, K. L., Robbins, A., Gumbrell, L., O'Malley, D., Tsiompanou, E., Shahbakhti, H., Webley, S., Hochhauser, D., Hilson, A. J., Blakey, D., and Begent, R. H. (2002) *Br. J. Cancer* **87,** 600–607
54. Spencer, D. I., Robson, L., Purdy, D., Whitelegg, N. R., Michael, N. P., Bhatia, J., Sharma, S. K., Rees, A. R., Minton, N. P., Begent, R. H., and Chester, K. A. (2002) *Proteomics* **2,** 271–279